Incorporation of Imidazolium Cations into an Enantiomeric Tartrate Host Lattice: Designing New Nonlinear Optical Materials

J. Fuller and R. T. Carlin*

The Frank J. Seiler Research Laboratory, 2354 Vandenberg Dr., Suite 2A35, United States Air Force Academy, Colorado 80840

L. J. Simpson and T. E. Furtak

Department of Physics, Colorado School of Mines, Golden, Colorado 80401

Received November 29, 1994. Revised Manuscript Received March 1, 1995[⊗]

A series of salts with nonlinear optical properties were synthesized using a single enantiomer of the tartrate anion to construct a host lattice for various imidazolium guest cations. The enantiomeric nature of the tartrate host lattice ensures a noncentrosymmetric salt structure and provides an efficient synthetic route to novel frequency-doubling materials. X-ray single-crystal structures, second harmonic generation (SHG) efficiencies, and refractive indexes were determined for seven such salts having different ring substitutions on the imidazolium guest molecule. Second harmonic generation efficiencies for the seven salts range from 0.3 to 2.2 times that of *d*-tartaric acid alone; thus, the imidazolium guest provides a distinct contribution to the total SHG response. A salient feature observed in the crytal structure of all salts is the extensive hydrogen bonding between tartrate units, forming a cross-linked tartrate chain lattice, and between the imidazolium guest and the tartrate host lattice. In addition, structural correlation to the nonlinear optical response shows that higher SHG efficiencies are realized when the imidazolium molecular plane is oriented in a parallel fashion to the tartrate chains.

Introduction

Systematic structure–property correlation studies have been applied to a range of chemical and biochemical systems including stereochemical reaction path investigations,[1,2] nonlinear optics,[3,4] magnetic susceptibility studies,[5] molecular recognition properties,[6] and enzyme–substrate model reactions.[7] These studies attempted to correlate structural features, such as hydrogen bonding, torsional angles, or packing dynamics, to a specific physical or chemical property that could then be further enhanced through structural modifications. An excellent series of reviews and articles on structure–property correlations in organic systems has recently appeared in *Chemistry of Materials* dedicated to the seminal work of Margaret C. Etter.[8]

The area of nonlinear optical (NLO) materials capable of second harmonic generation (SHG) has received a great deal of this attention due to the commercial importance of these materials in the fields of optical communication, signal processing, sensing, and instrumentation.[9] Systematic structural investigations of classes of NLO materials have included chiral pyrrolo-[1,2-*a*]quinolines,[10] dihydrogenphosphate salts,[3] 2-amino-5-nitropyridinium salts,[11] and stilbazolium salts.[4] These studies were aimed at correlating structural properties to the nonlinear responses with the ultimate goal being the possibility of "tuning" the structure to enhance the nonlinear properties. In addition, of particular relevance to the study discussed in this paper is the work of Velsko et al., who have combined an extensive synthetic effort with eloquent optical measurements to achieve a statistical approach to identifying chiral salts of amino acids and carboxylic acids for harmonic generation.[12–14] In all the above investigations, organic salts have proven to be a particularly fruitful area of research, leading to enhanced SHG efficiencies[15] and commercially viable NLO materials such as deuterated L-arginine phospate (*d*-LAP).[16]

[⊗] Abstract published in *Advance ACS Abstracts,* April 15, 1995.

(1) Kaftory, M.; Nugiel, D. A.; Biali, S. E.; Rappoport, Z. *J. Am. Chem. Soc.* **1989**, *111*, 8181–8191.
(2) Bürgi, H. B. *Angew. Chem., Int. Ed. Engl.* **1975**, *14*, 460–473.
(3) Aakeröy, C. B.; Hitchcock, P. B.; Moyle, B. D.; Seddon, K. R. *J. Chem. Soc., Chem. Commun.* **1989**, 1856–1859.
(4) Marder, S. R.; Perry, J. W.; Tiemann, B. G.; Marsh, R. E.; Schaefer, W. P. *Chem. Mater.* **1990**, *2*, 685–690.
(5) Kawata, T.; Uekusa, H.; Ohba, S.; Furukawa, T.; Tokii, T.; Muto, Y.; Kato, M. *Acta. Crystallogr.* **1992**, 253–261.
(6) Etter, M. C.; Urbańczyk-Lipkowska, Z.; Zia-Ebrahimi, M.; Panunto, T. W. *J. Am. Chem. Soc.* **1990**, *112*, 8415–8426.
(7) Holmes, R. R.; O. Day, R.; Yoshida, Y.; Holmes, J. M. *J. Am. Chem. Soc.* **1992**, *114*, 1771–1778.
(8) See articles and reviews in: *Chem. Mater.* **1994,** *6*, 1087–1462.
(9) Eaton, D. F. *Science* **1992**, *253*, 281–287.
(10) Kelderman, E.; Verboom, W.; Engbersen, J. F. J.; Harkema, S.; Heesink, G. J. T.; Lehmusvaara, E.; van Hulst, N. F.; Reinhoudt, D. N. *Chem. Mater.* **1992**, *4*, 626–631.
(11) Pecaut, J.; Masse, R. *Acta. Crystallogr.* **1993**, *B49*, 277–282.
(12) Velsko, S. P. In *Materials for Nonlinear Optics: Chemical Perspectives*; Marder, S. R., Sohn, J. E., Stucky, G. D., Eds.; American Chemical Society: Washington, DC, 1990; Vol. 455, pp 343–359.
(13) Eimerl, D.; Velsko, S.; Davis, L; Wang, F. *Prog. Cryst. Growth Charact.* **1990,** *20*, 59–113.
(14) Velsko, S. P.; Davis, L. E.; Wang, F.; Eimerl, D. *SPIE* **1988,** *971*, 113–117.
(15) Marder, S. R.; Perry, J. W.; Yakymyshyn *Chem. Mater.* **1994,** *6*, 1137–1147.
(16) Barker, C. E.; Eimerl, D.; Velsko, S. P. *J. Opt. Soc. Am. B* **1991,** *8*, 2481–2492.

0897-4756/95/2807-0909$09.00/0 © 1995 American Chemical Society

Engineering NLO materials for optimal SHG efficiency requires several important physical and structural requirements be met and optimized. The parameters that must be engineered into the materials are nonzero optical susceptibility coefficients (d_{ijk}) or noncentrosymmetry, transparency at the fundamental and second harmonic wavelengths, birefringence large enough to allow for phase matching, high optical damage thresholds, and good physical properties (e.g., high melting point, easy crystal growth, mechanical durability, machinable, etc.). In view of the number of requirements, much current research has focused on organic materials because of their relative ease of synthesis and structural modification.

The requirement of noncentrosymmetry for SHG has been successfully designed into several organic systems using a number of strategies. The most obvious is the use of a single enantiomer of a chiral component which then guarantees crystallization into an acentric space group.[12,17] A more subtle approach uses molecular influences, such as hydrogen bonding, to help direct the formation of molecular aggregates with predictable noncentrosymmetric patterns.[8,18] Brute force noncentrosymmetry is commonly achieved by incorporating an appropriate organic guest molecule in a host polymer matrix and applying an electric field to align the guest dipoles; this produces a temporary SHG response which is lost over time due to relaxation of the guest–host structure.[19] A similar solid-state chemistry approach employs inorganic molecular sieve hosts, such as ALPO-5, to provide an acentric environment for 2-methyl-*p*-nitroaniline guests.[20]

An organic enantiomeric guest–host system is described in this paper. The guest molecule is an aromatic imidazolium cation that can be tailored through ring substitution and hydrogen-bonding ability to enhance the NLO response. The host lattice is constructed with an enantiomeric monohydrogen tartrate anion that fulfills the noncentrosymmetric requirement and provides a constant contribution to the SHG efficiency. The tartrate anion also serves to tie the guest molecule into the acentric lattice through hydrogen bonding thus forming a complex three-dimensional hydrogen bonded network. These salts possess many of the desired NLO characteristics—noncentrosymmetry, wide transparency window, phase matchablility, high melting points, and simple crystal growth procedures.

Experimental Section

The salts were prepared by mixing stoichiometric amounts of the appropriate imidazole with an enantiomer of tartaric acid. All materials were purchased from Aldrich and were used without further purification. Capillary melting point measurements were made on a Melttemp apparatus. A Rigaku Model DMAX-B powder diffractometer was employed to record the diffraction patterns of the bulk salt preparation. These experimental powder patterns were compared to powder patterns generated from the single-crystal data to ensure the single-crystal structure was representative of the bulk sample used in the SHG measurement. Refractive index measurements were performed by McCrone Associates (Westmont, IL) using the sodium line by either the immersion or spindle stage technique. A Hewlett Packard 8452A diode array spectrophotometer was employed to record the UV–vis solution spectra of all salts.

Second harmonic measurements were performed using the Kurtz and Perry technique.[21] All materials were particle sized using a set of microsieves (Fisher Scientific). Urea (99%, Aldrich) and α-quartz (Valpey-Fisher) were used as standards. The α-quartz was purchased as a large single crystal (~1 lb) and was crushed and particle sized. The sample cell consisted of a depression microscope slide (Fisher) covered with a flat microscope slide. For the larger particle sizes, a depression slide with a deeper well was used to ensure that the particles were not crushed. A pulsed Nd:YAG laser (Quanta-Ray DCR 10, 10 Hz repetition rate, 20 ns pulsewidth, 10 mJ pulse energy, 1064 nm wavelength) provided the incident radiation. This was directed into one opening of an integrating sphere. The integrating sphere was mounted on a high-precision translation stage and the sample was mounted on the side opposite to the entrance hole. The incident light was perpendicular to the glass slide and was focused to an area of approximately 1 cm^2. The second harmonic radiation was detected through a third opening in the integrating sphere, located halfway between the other two openings. This arrangement enabled comparison of the SHG efficiency of a salt to a standard while minimizing the effects of sample positioning and finite detection angles. The detection system consisted of a combination of a short-wavelength-passing filter and a 1/4 m monochromator (Kratos GM250, 3.3 nm bandpass), coupled to a photomultiplier (Hamamatsu R212). The signal was processed with a large-bandwidth preamplifier and a boxcar averager (SRS SR250), whose temporal window was set to collect the entire pulse. The resulting output was monitored with an analog voltmeter. Data for several guest–host salt samples and an appropriate standard (α-quartz or urea) were collected in a single session. The SHG efficiency of each sample was calculated by ratioing its voltmeter response to that of the standard recorded at intervals during data collection. The response of the standard remained essentially constant during each data collection session. Several samples were remeasured during different data collection sessions to ensure the SHG efficiency was reproducible. Although the voltmeter response for the standards varied for each data collection session, the calculated SHG efficiency of each guest–host salt sample was reproducible within 10% from session to session. All SHG efficiencies are reported as the experimentally determined ratio of SHG intensity of the salt to that of *d*-tartaric acid, $I^{2\omega}/I^{2\omega}{}_{d\text{-tartaric acid}}$, unless stated otherwise.

$C_7N_2O_6H_{10}$ (1). Imidazole (0.214 g, 0.003 mol) was dissolved in 15 mL of water. D-Tartaric acid (0.427 g, 0.003 mol) was added, and the mixture was heated until all solids had dissolved. The solvent was removed by rotary evaporation to yield **1** as a white crystalline solid; melting point 213–214 °C. Crystals suitable for X-ray diffraction were obtained by slow evaporation of a saturated methanol solution.

$C_9N_2O_6H_{12}$ (2). 1-Vinylimidazole (0.413 g, 0.0044 mol) was dissolved in 20 mL of hot water. D-Tartaric acid (0.609 g, 0.0041 mol) was added and dissolved. Crystals of **2** suitable for X-ray analysis were obtained by slow evaporation of the aqueous solvent; melting point 120–122 °C.

$C_8N_2O_6H_{12}$ (3). 2-Methylimidazole (1.373 g, 0.0167 mol) was dissolved in a 20 mL 1:1 mixture of water:methanol. D-Tartaric acid (2.480 g, 0.165 mol) was added, and the mixture was heated until all solids were dissolved. The solution was allowed to evaporate yielding large, colorless, single crystals of **3** suitable for X-ray diffraction; melting point 203–204 °C.

$C_8N_2O_6H_{12}$ (4). 1-Methylimidazole (0.933 g, 0.0114 mol) was dissolved in 15 mL of a warm 1:1 water:methanol mixture. D-Tartaric acid (1.630 g, 0.0109 mol) was added and dissolved. The solvent mixture was removed by rotary evaporation, and the resulting solid was dried under vacuum at 75 °C for 24 h.

(17) Aakeröy, C. B.; Hitchcock, P. B.; Seddon, K. R. *J. Chem. Soc., Chem. Commun.* **1992**, 553–555.
(18) Etter, M. C.; Frankenbach, G. M. *Chem. Mater.* **1989**, *1*, 10–12. Etter, M. C. *J. Phys. Chem.* **1991**, *95*, 4601–4610.
(19) Brower, S. C.; Hayden, L. M. *Appl. Phys. Lett.* **1993**, *63*, 2059–2061.
(20) Cox, S. D.; Gier, T. E.; Stucky, G. D.; Bierlein, J. *J. Am. Chem. Soc.* **1988**, *110*, 2986–2987.
(21) Kurtz, S. K.; Perry, T. T. *J. Appl. Phys.* **1968**, *39*, 3798–3813.

Table 1. X-ray Structure Determination Summary

	1	2	3	4	5	6	7
				Crystal Parameters			
formula	$C_7N_2O_6H_{10}$	$C_9N_2O_6H_{12}$	$C_8N_2O_6H_{12}$	$C_8N_2O_6H_{12}$	$C_{15}N_2O_7H_{16}$	$C_9N_2O_6H_{14}$	$C_{13}N_2O_9H_{14}$
fw	218.2	244.2	232.2	232.2	336.3	246.2	346.3
cryst syst	monoclinic	monoclinic	monoclinic	monoclinic	triclinic	monoclinic	orthorhombic
space group	$P2_1$	$P2_1$	$P2_1$	$P2_1$	$P1$	$P2_1$	$P2_12_12_1$
a, Å	7.595(2)	4.891(1)	4.739 (1)	7.609(2)	5.127(1)	7.739(2)	7.208(1)
b, Å	6.981 (1)	17.337(3)	16.281(3)	7.587(2)	7.673(2)	8.123(2)	9.372(2)
c, Å	9.017(3)	6.544(1)	6.746(1)	9.414(2)	9.986(2)	17.879(4)	22.927(5)
α, deg					76.94(3)		
β, deg	101.51(3)	100.34(3)	100.895(3)	105.24(3)	81.22(3)	95.03(3)	
γ, deg					79.77(3)		
V, Å^3	468.5(2)	545.94(17)	511.12(16)	524.4(2)	374.04(14)	1119.7(5)	1548.7(5)
Z	2	2	2	2	1	4	4
cryst dimens, mm	0.1 × 0.4 × 0.8	0.4 × 0.4 × 0.3	0.2 × 0.4 × 0.8	0.15 × 0.1 × 0.4	0.5 × 0.4 × 0.2	0.2 × 0.4 × 0.8	0.4 × 0.4 × 0.5
cryst color	colorless	white	colorless	colorless	brown	colorless	brown
D(calc), g cm^{-3}	1.547	1.486	1.509	1.471	1.493	1.461	1.485
absorp coeff, mm^{-1}	0.128	0.118	0.122	0.119	0.112	0.116	0.119
temp, K	296	296	296	296	296	296	296
				Data Collection			
radiation	Mo Kα	(λ = 0.710 73 Å)					
2θ scan range, deg	3–50	3–60	3–45	3–60	3–45	3–50	3–45
data collected (h, k, l)	±9, +8, +10	+5, ±20, ±7	+5, +19, ±8	-1 +8, −1 +8, ±11	±5, ±8, +10	+8, +8, ±19	+7, +10, +24
no. of reflns measd	958	1075	1040	1399	1061	2301	1196
no. of independent reflns	900	1040	929	1136	1061	1832	1196
no. obsd reflns $F_o \geq 4\sigma(F_o)$	817	933	865	652	1017	1740	1011
R(merg), %	1.16	2.00	1.34	3.28	0.00	1.63	0.00
				Refinement			
R	0.0411	0.0491	0.0315	0.0573	0.0301	0.0274	0.0317
wR	0.0553	0.0711	0.0450	0.0600	0.0413	0.0368	0.0399
$w = 1/[\sigma^2(F) + 0.0000F^2]$	0.0016	0.0018	0.003	0.0009	0.0004	0.0005	0.0005
Δ/ϱ_{max} = e Å^{-3}	0.23	0.18	0.19	0.28	0.26	0.18	0.15
GOF	1.23	1.40	0.80	1.21	1.83	1.13	1.30

The resulting white salt was gummy and proved difficult to recrystallize. A quantity of the salt in excess of its solubility limit was placed in a 5 mm NMR tube containing approximately 1 mL of acetonitrile. The tube was capped and partially inserted in a sand bath placed on a hot plate which established a temperature gradient of 20–100 °C within the sand bath. Internal convection within the saturated acetonitrile solution resulted in the deposition of crystals of **4** (0.4 × 0.4 × 0.6 mm) suitable for X-ray diffraction on the walls of the NMR tube within 5 h; melting point 98–101°C.

$C_{15}N_2O_7H_{16}$ (5). 4′-(Imidazol-1-yl)acetophenone (0.138 g, 0.000 74 mol) was dissolved in 15 mL of hot water. D-Tartaric acid (0.112 g, 0.000 75 mol) was added and dissolved. The resulting orange liquid was slowly allowed to evaporate yielding large, transparent, brown crystals in 2 weeks. Crystals of **5** suitable for X-ray analysis were obtained without further recrystallization; melting point 150–153 °C.

$C_9N_2O_6H_{14}$ (6). 2-Ethylimidazole (0.54 g, 0.0056 mol) was dissolved in 15 mL of hot water. D-Tartaric acid (0.839 g, 0.0056 mol) was added and dissolved. The solution was allowed to slowly evaporate yielding large, colorless crystals in 1 week. Crystals of **6** suitable for X-ray analysis were obtained without further recrystallization; melting point 41–43 °C.

$C_{13}N_2O_9H_{14}$ (7). 4′-(Imidazol-1-yl)phenol (0.148 g, 0.0009 mol) was dissolved in 15 mL of hot water. D-Tartaric acid (0.133 g, 0.0009 mol) was added and dissolved. The solvent was removed by rotary evaporation yielding a light brown solid. Crystals of **7** suitable for X-ray analysis were obtained by slow evaporation of a saturated acetone solution; melting point 152–154 °C.

X-ray Data Collection, Structure, and Refinement. All crystals were mounted in sealed glass capillary tubes (Charles Supper). Data for **1** and **4–7** were collected on a Siemens R3m/V diffractometer using cell parameters determined from 25 reflections between 10 and 25 2θ. Data for **2** and **3** was collected on a Siemens P4 diffractometer using cell parameters determined from 50 reflections 10–25 2θ.[22] All data was corrected for Lorentz and polarization effects, but no correction was made for absorption. Three check reflections were monitored after every 100 reflections to check for crystal decay or slippage.

All crystallographic calculations were carried out using Siemens SHELXTL-PC Version 2.0a.[23] The structure was solved by direct methods and refined by full-matrix least-squares techniques. The absolute structure was not determined and was presumed to be that of the original starting enantiomer. Crystal parameters and refinement information for **1–7** are tabulated in Table 1. Positional parameters for **1–7** are provided as supplementary material. Located hydrogens were isotropically refined, and all other hydrogens were placed in idealized positions. The hydrogen on the carboxylate group was unambiguously determined from electron difference maps. Because all of the hydrogen positions could not be located, the criterion used to identify hydrogen bonds in the structure is the X···Y distance in X–H···Y must be smaller than the sum of the van der Waals radii of X and Y and the X–H···Y angle must be greater than or equal to 90°.[24] Hydrogen bonds in the structure are tabulated in Table 2 where both X···Y and H···Y distances are reported along with X–H···Y angles. Molecular structures of **1–7** with the labeling schemes are shown in Figures 1 and 2 with 50% probability thermal ellipsoids. The graphics package included in Siemens SHELXTL-PC[23] was used to generate the figures.

Results and Discussion

It has been pointed out that tartrate salts possess a number of NLO favorable properties.[12,17] Specifically,

(22) Siemens (1993) P4/RA XSCANS diffractometer program.
(23) Siemens (1990) SHELXTL-Plus/PC Version 4.1 Siemens Analytical X-ray Instruments Inc., Madison, WI.
(24) Huheey, J. E. In *Inorganic Chemistry*, 3rd ed.; Harper & Row: New York, 1983; p 256.

Table 2. Host···Host and Host···Guest Interactions, X···Y (Å), H···Y (Å), and X–H···Y (deg) Hydrogen Bond Distances and Angles[a]

interaction	1	2	3	4	5	6 ($Z = 4$)	7
carboxylate···carboxylate O···O, O···H, O–H···O	2.516, 1.868, 123.5	2.455, 1.616, 168.7	2.486, 1.455, 169.0	2.477, 1.268, 161.0	2.617, 1.787, 165.0	2.505, 1.679, 163.3 2.616, 1.773, 171.0	2.586, 1.748, 168.6
carboxylate···hydroxyl O···O, O···H, O–H···O		3.103, 2.285, 161.8		2.893, 2.507, 108.6		2.853, 2.026, 164.2 2.749, 1.916, 165.9 2.643,1.793, 177.3 2.761, 1.911, 177.8	
hydroxyl···hydroxyl O···O, O···H, O–H···O	3.065, 2.248, 161.1		2.781, 1.824, 162.7	2.897, 2.109, 153.9			
carboxylate···NH O···N, O···H, O···H–N	2.737, 1.854, 166.1 3.044, 2.238, 148.9	2.703, 1.826, 164.1	3.117, 2.151, 138.2 2.690, 1.843, 115.9		2.621, 1.665, 173.3	2.719, 1.872, 156.0 2.806, 2.140, 130.1 2.780,1.905, 163.6	23891, 2.164, 137.3
carboxylate···CH O···C, O···H, O···H–C	3.046, 2.605, 108.4	3.143, 2.513, 123.2 3.325, 2.533, 139.9		3.145, 2.239, 156.9 3.255, 2.334, 160.5 3.191, 2.542, 125.0	3.122, 2.186, 164.6	3.220, 3.007, 94.0 3.314, 2.422, 154.4	
hydroxyl···NH O···N, O···H, O···H–N		3.150, 2.572, 122.6		2.904, 2.011, 131.3		2.881, 2.073, 148.9	
hydroxyl···CH O···C, O···H, O···H–C	3.198, 2.296, 156.3						

[a] Additional interactions: **5** cation···cation: 3.043, 2.539 and 3.015, 2.492 between O(1)···C(4) and O(1)···C(5) respectively. **7** cation···anion: 2.784, 1.936 and 2.947, 2.560 between O(1)···O(6) and O(1)···O(4) respectively. **7** anion···water (O···O): 2.761, 2.703, 2.813, 2.708 between O(23)···O(4), O(23)···O(3), O(24)···O(7), and O(24)···O(2) respectively.

these salts are colorless, transparent, and readily soluble and have generally high melting points. Thermal stability is particularly important for the construction of devices capable of tolerating operational heating. In addition, the simplicity of the synthetic routes to these salts makes possible rapid preparation and SHG screening. Moreover, the variety and quantity of cations that can be combined with the tartrate anion makes tuning of select properties feasible. For example, the ability to tune the refractive indexes through cation choice allows these tartrate salts to be incorporated into organic polymers as SHG-active composites; refractive index matching is critical in this application.[3]

The enantiomeric monohydrogentartrate molecule has a predictable structure comprised of head to tail carboxyl and carboxylate anion groups that form a helical chain arrangement held together by moderate to strong hydrogen bonds.[25,26] Both the hydroxyl oxygens and the carbonyl oxygens not involved in forming the helical chain are free to participate in hydrogen bonding with tartrate molecules in other chains, thus forming a cross-linked network. When only one enantiomer of the tartrate anion is used to form the network, as in this study, the acentric "host" network should contribute to the total NLO susceptibility of the salt; however, this component may be relatively small as is evidenced by the modest SHG efficiency of *d*-tartaric acid.[27] Additionally, based on absolute weight or volume of the salt, the quantity of tartrate present is diluted by the presence of the cations, decreasing further the tartrate contribution to the total SHG efficiency. However, the tartrate SHG contribution calculated on a mole of tartrate per unit volume of salt should remain relatively constant. In fact, the expected SHG contribution from the tartrate host can be estimated from eq 1 in which the *d*-tartaric acid SHG efficiency is scaled by the effective mole per unit volume of the tartrate molecule in the salt.

$$\text{estimated tartrate SHG contribution} = (d\text{-tartaric acid SHG})\left[\frac{\varrho_{\text{salt}}/MW_{\text{salt}}}{\varrho_{d\text{-tart}}/MW_{d\text{-tart}}}\right] \quad (1)$$

In the above equation, ϱ and MW are the density and molecular weight, respectively, of the tartrate salt or of *d*-tartaric acid. The SHG value of *d*-tartaric acid is experimentally measured and normalized to 1 unless stated otherwise.

Despite the modest SHG efficiencies expected from the tartrate lattice alone, several enantiomeric tartrate salts exhibit SHG efficiencies comparable to α-quartz and in some cases urea.[17,27,28] These increases in SHG efficiency may be due to a property of the cationic guest molecule or perhaps to the interactions or alignment of the guest molecule with the tartrate host lattice. For example, previous work on hydrazonium tartrate salts suggests that the SHG response is induced by the nonlinear electronic polarizability of the hydrogen bonds between the cation and anion.[27] Therefore, in this case,

(25) Okaya, Y.; Stemple, N. R.; Kay, M. I. *Acta. Crystallogr.* **1966**, *21*, 237–243.
(26) Hope, H.; De La Camp, U. *Acta. Crystallogr.* **1972**, *A28*, 201–207.
(27) Delfino, M.; Jacco, J. C.; Gentile, P. S.; Bray, D. D. *J. Solid State Chem.* **1977**, *21*, 243–251.
(28) Zyss, J.; Pecaut, J.; Levy, J. P.; Masse, R. *Acta. Crystallogr.* **1993**, *B49*, 334–342.

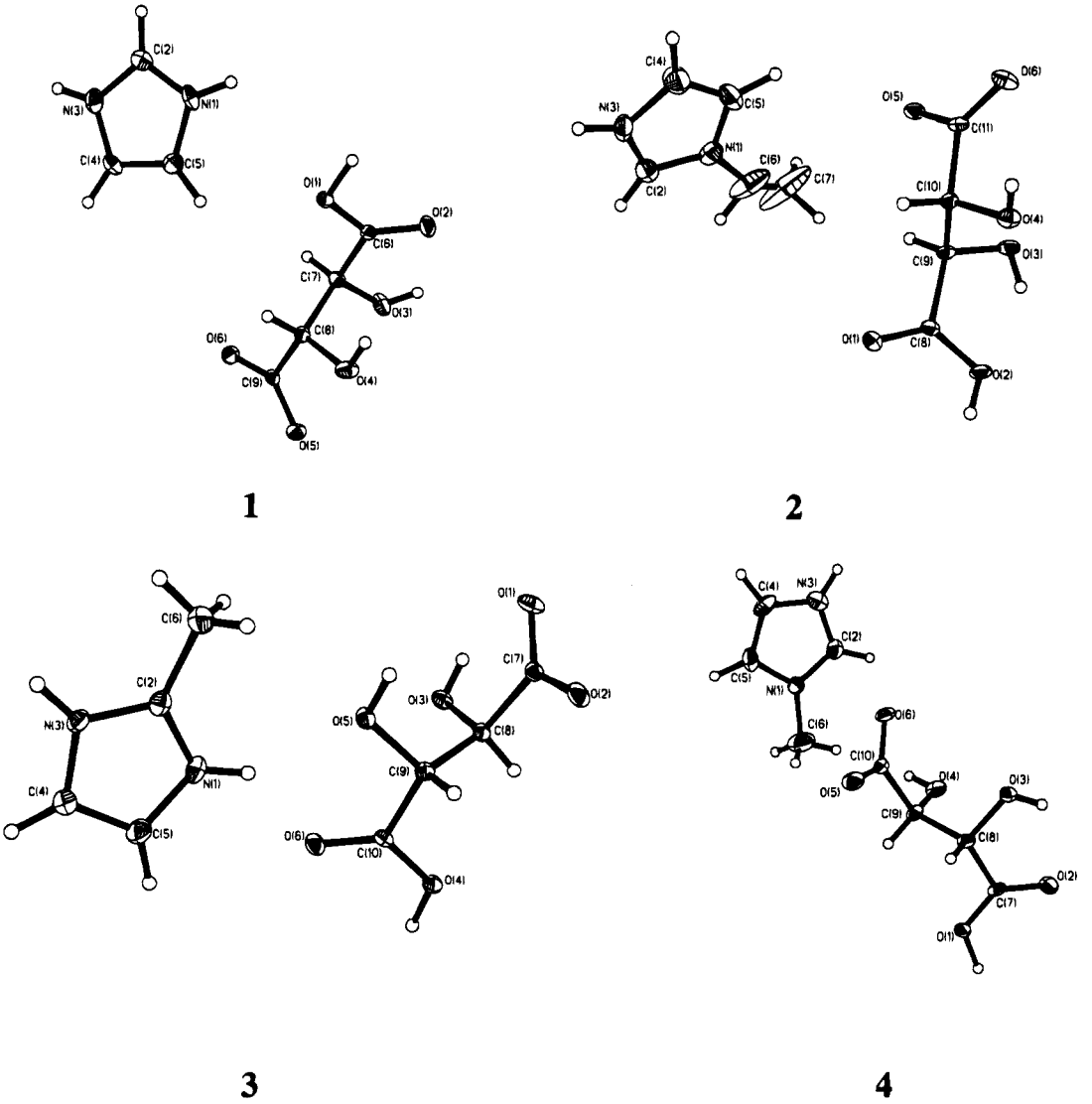

Figure 1. Imidazolium *d*-tartrate (1), 1-vinylimidazolium *d*-tartrate (2), 2-methylimidazolium *d*-tartrate (3), and 1-methylimidazolium *d*-tartrate (4).

the host–guest hydrogen-bond interactions are evidently influencing the SHG efficiency of the salt. The guanidinium tartrate salt also has been reported to have an improved NLO response over the enantiomeric *d*-tartaric acid.[28] In this example, the cations are again involved in extensive hydrogen bonding with the anionic host network, but the cationic network contains pseudocenters of symmetry which lower the overall SHG ability of the salt compared to that which might be expected from the urea-like guanidinium molecule.[28] These two examples emphasize the importance of examining the hydrogen bond interactions of the salt, as well as the orientation of the guest molecule to the host lattice when considering the SHG ability of designed NLO materials.

Second Harmonic Generation. For maximum nonlinear optical efficiency, it is desirable to have a material that does not absorb either the fundamental or the harmonic wavelengths. UV–visible spectra were recorded for 0.02 M salt solutions. All the salts in solution had no absorption bands in the region of frequency doubling, and five of the seven materials in this study were colorless crystals. The five colorless solids are not expected to have absorption bands in the 532 nm region and are therefore acceptable frequency-doubling materials.

It has been shown by Miller that the refractive index is directly proportional to the second order nonlinear optical response.[29] This correlation in refractive index, a linear optical property, and the nonlinear optical property of second harmonic generation is known as Miller's rule. Kurtz and Perry noted that the dependence between refractive index and second harmonic intensity relates in the following way:

$$I^{2\omega} \propto [n^2 - 1/n + 1]^6 \qquad (2)$$

where n is the refractive index of the sample.[30] In Table 3 are the calculated Miller's rule predictions. The general trend is that salts with enhanced SHG efficiencies have higher predicted (eq 2) SHG efficiencies. The exceptions to this observation are salts **6** and **7**, which have significantly lower SHG efficiencies than what Miller's rule would predict. This deviation in expected SHG ability will be discussed in more detail in the following sections.

(29) Miller, R. C. *Appl. Phys. Lett.* **1964**, *5*, 17–19.
(30) Bourhill, G.; Mansour, K.; Perry, K. J.; Khundkar, L.; Sleva, E. T.; Kern, R.; Perry, J. W. *Chem. Mater.* **1993**, *5*, 802–808.
(31) Weast, R. C.; Astle, M. J. In *CRC Handbook of Chemistry and Physics;* CRC Press: Boca Raton, FL, 1981–1982; Vol. 62.

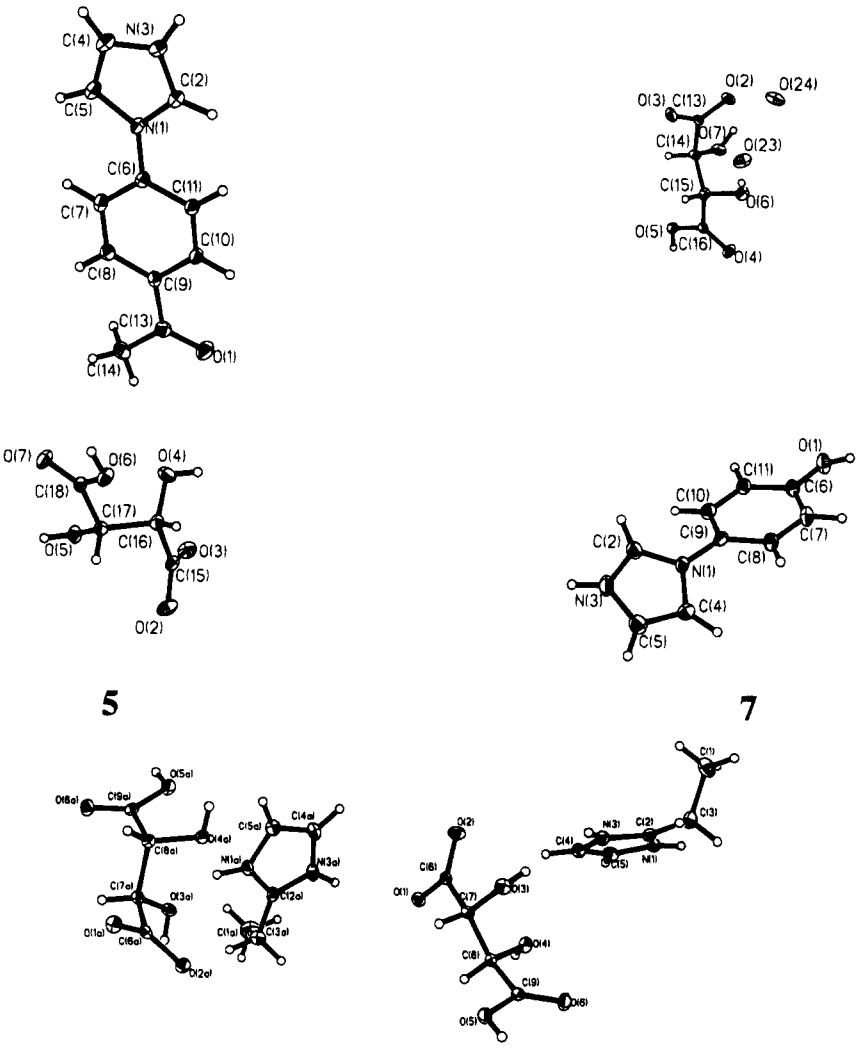

Figure 2. 1-Acetophenoneimidazolium *d*-tartrate (5), 2-ethylimidazolium *d*-tartrate (6), and 1-phenolimidazolium *d*-tartrate (7).

Table 3. Measured Properties of 1–7

salt	refractive indices[a] α min	β	γ max	calcd contribution of tartrate to SHG efficiency[b,c]	phase matchability	$I^{2\omega}/I^{2\omega}_{d\text{-tartaric acid}}$	Miller's rule prediction[d,e]
1	1.520	1.578	1.660	0.607	yes	2.23	5.61
2	1.556	1.579	1.605	0.521	yes	1.99	3.31
3	1.537	1.565	1.592	0.556	yes	1.37	2.91
4	1.527		1.571	0.538	yes	1.43	2.52
5	1.525	1.596	1.678	0.376	yes	1.24	6.55
6	1.540	1.557	1.578	0.507	no	0.44	2.52
7	1.551	1.584	1.620	0.368	yes	0.30	3.84

[a] α, β, and γ from spindle stage measurement or min/max from immersion technique. [b] Estimated tartrate SHG contribution from eq 1. [c] Density of *d*-tartaric acid is 1.7598.[31] [d] $[n^2 - 1/n + 1]^6_{\text{salt}}/[n^2 - 1/n + 1]^6_{d\text{-tartaric acid}}$. [e] n is the isotropic refractive index: $n_{(d\text{-tartaric acid})} = 1.4955$.[31]

The determination of phase-matchability was possible from the particle size measurements made on <35, 35–45, 45–60, 60–80, 80–120, 120–170, 170–230, and >230 μm particle sized salts. The results of these experiments were plotted as in Figure 3, and the phase matchability was determined and are tabulated in Table 3. Representative plots of a phase-matchable, **1**, and a non-phase-matchable, **6**, salts are provided in Figure 3.

Crystal Structure Packing Dynamics. Table 3 lists the estimated tartrate contribution to the total SHG efficiency of the salt based on eq 1. Note that in most cases, with the exception of **6** and **7**, the salts have a larger relative SHG ability than what is predicted from the presence of the tartrate lattice alone. This suggests that the cations result in an enhancement of SHG efficiency in five of the seven salts examined here. For **6** and **7**, the predicted SHG contribution of the tartrate host lattice is very close to the experimental SHG efficiency of the salt. One possible explanation for the lower SHG efficiency in these two cases is that the space group or the number of asymmetric units is not optimized for these two salts; $Z = 4$ for **6**, while **7** is orthorhombic and is hydrated. However, an alternate explanation is that the packing of the cation with

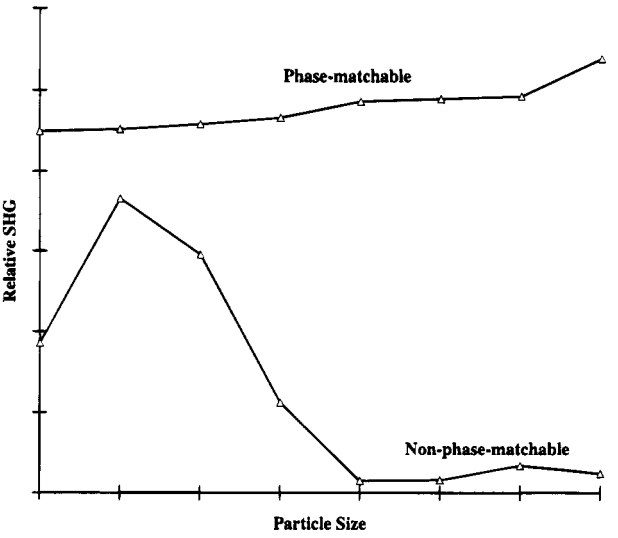

Figure 3. Representative plots of a phase-matchable salt, imidazolium *d*-tartrate, and a non-phase-matchable salt, 2-ethylimidazolium *d*-tartrate.

Table 4. Defined Geometry of Guest and Host Molecules to Crystallographic Axes (deg)

	1	2	3	4	5	6	7
angles between host chain and axis							
a	0	100.3	100.9	0	79.8	0, 0	0
b	90	90	90	90	0	90, 90	90
c	101.5	0	0	105.2	76.9	85.0,95.0	90
angles between guest plane and axis							
a	20.4	45	45.7	9.7	34.7	65.3, 65.9	75.9
b	67.8	26.4	39.8	73.6	26.5	23.1, 24.0	11.7
c	4.1	24.4	24.3	10	37.7	3.7, 1.8	7.8
piercing point[a]	20.4	24.4	24.3	9.7	26.5	65.9, 65.3	75.9

[a] The angle formed by the intersection of the plane of the imidazolium ring and the tartrate chain.

respect to the host tartrate lattice is somehow different for these two salts compared to the others in this series.

To analyze the packing dynamics of the host–guest interaction, it is first necessary to define the packing geometry of the guests and hosts with respect to the crystallographic axes. Listed in Table 4 are the angles between the crystallographic axes and the anionic chain (defined by the interlinked tartrates running parallel to an axis) and between the crystallographic axes and the cationic planes (defined by the plane of the imidazolium cation). From this table, it is apparent that the tartrate chain runs along the *a* axis in **1**, **4**, **6**, and **7** and along the *c* axis in **2** and **3**. It should be noted that for salts **2** and **3**, the tartrate chain is defined as a carboxyl- or carboxylate-to-hydroxyl linkage and not a carboxyl-to-carboxylate chain as in the other salts. For these two salts, the carboxyl to carboxylate chain runs along a diagonal through the crystal. It is hoped that by defining the host lattice as a chain that runs parallel to an axis, rather than along a diagonal, the arrangement of the molecules can be more easily envisioned.

The angle formed by the alignment of the guest molecule to the host chain was determined by first defining the imidazolium cation as a plane. Next, two tartrate anions in adjacent unit cells were linked together by a line command in the SHELXTL graphics program, and the angle formed between the plane and the line was calculated within the SHELXTL program.[23]

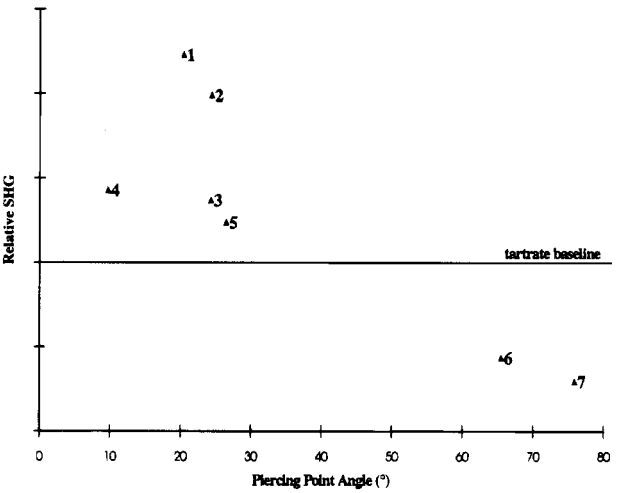

Figure 4. Plot of relative second harmonic signal vs piercing point angle.

This angle is defined as the piercing point and is listed at the bottom of Table 4. The piercing point angle clearly defines the orientation of the guest molecule to the host lattice.

Figure 4 is a plot of the calculated piercing point versus $I^{2\omega}/I^{2\omega}_{d\text{-tartaric acid}}$ for the salts. For salts with enhanced SHG over tartaric acid, the plane of the guest molecules is aligned nearly parallel with the tartrate chain, i.e., low piercing point angles. The two salts with SHG efficiencies approaching that calculated from eq 1 have higher piercing point angles with the guest being almost perpendicular to the host. This would imply that for the perpendicular alignment, the salt behaves as a diluted tartrate unit, i.e., the presence of the cation has no direct influence on the SHG efficiency. Although an optimum alignment of molecules with the solid-state dielectric axes has been well established for SHG,[32,33] we are not aware of any studies demonstrating a similar optimum alignment for guest molecules relative to a

(32) Zyss, J.; Oudar, J. L. *Phys. Rev. A* **1982**, *26*, 2028–2048.
(33) Based on work presented in ref 32, an effort was made to correlate SHG efficiency with the angle between the imidazolium cation, or its estimated dipole, and the Y (monoclinic) or Z (orthorhombic) dielectric axes; however, no such correlation could be found.

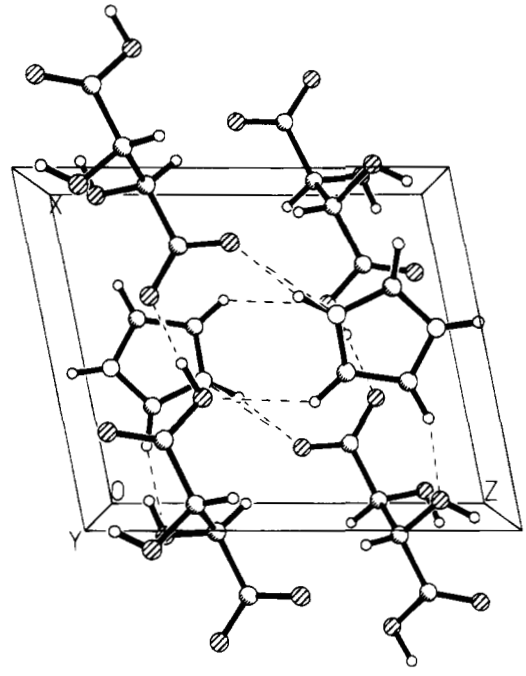

Figure 5. Imidazolium *d*-tartrate, view down *b* axis.

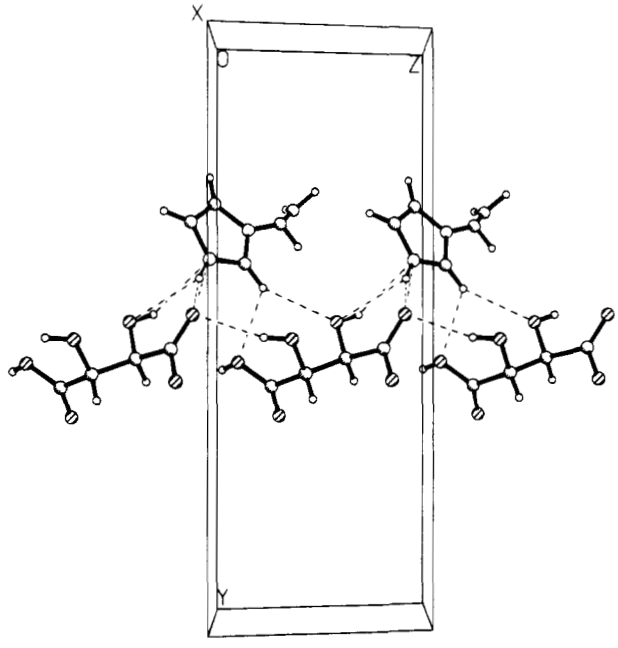

Figure 6. 1-Vinylimidazolium *d*-tartrate, view down *a* axis.

linear host lattice. An overly simplified, but perhaps valid, explanation is that the parallel guest–host arrangement aligns the aromatic delocalized electron density of the cation with the conjugated SHG-active carboxylate functional groups on the tartrate host.[12] Figures 5–11 are views of the salts which illustrate the parallel versus perpendicular alignment of the host–guest structure. Figure 4, therefore, illustrates that an enhancement of the SHG efficiency results when the guest cation plane closely parallels the host chain, while the perpendicular arrangement of the guest to host gives no enhancement over the tartrate host lattice alone.

Influence of Hydrogen Bonding on Alignment of Host–Guest. Directed hydrogen-bonding interactions offers a powerful tool in designing NLO materi-

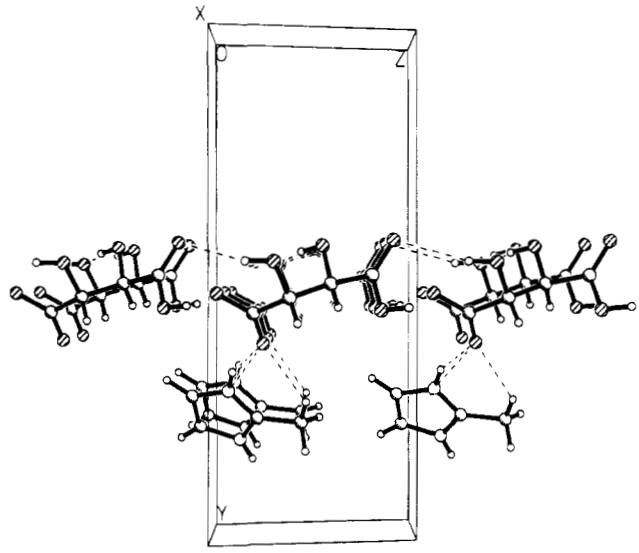

Figure 7. 2-Methylimidazolium *d*-tartrate, view down *a* axis.

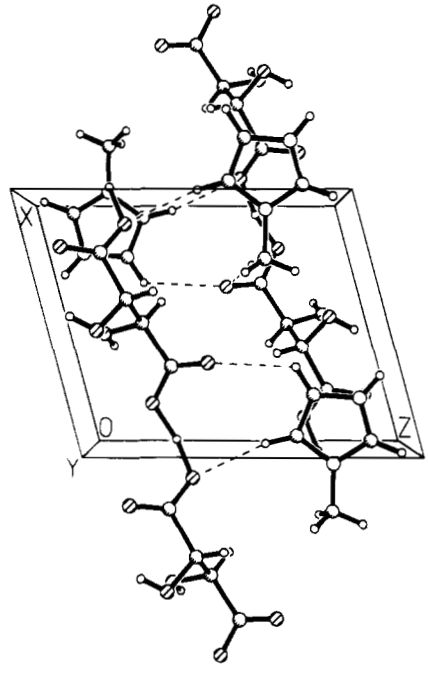

Figure 8. 1-Methylimidazolium *d*-tartrate, view down *b* axis.

als.[34] When a hydrogen bond forms between a guest and host pair, it can direct the configuration of the pair with as much control as a covalent bond.[6] The strength of the hydrogen bond interaction enhances the stability of the host–guest pair. In addition, a strong hydrogen bond between host molecules can increase the structural stability of the host lattice thus creating a strong support lattice for the guest molecule. A hydrogen-bond chain is inherently acentric when it is covalently bonded to an electronegative atom, X, and associated with another less-electronegative atom, Y. Therefore, when multiple hydrogen-bond sites are involved, as in the case of the imidazolium tartrate salts, the possibility exists for creating an acentric multidimensional hydrogen-bond network.[18]

All of the enantiomeric tartrate imidazolium salts surveyed exhibited some SHG response (Table 5). The

(34) Garcia-Tellado, F.; Geib, S. J.; Goswami, S.; Hamilton, A. D. *J. Am. Chem. Soc.* **1991**, *113*, 9265–9269.

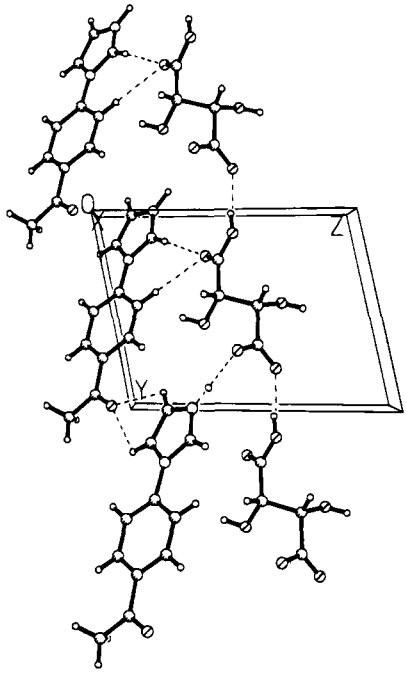

Figure 9. 1-Acetophenoneimidazolum *d*-tartrate, view down *a* axis.

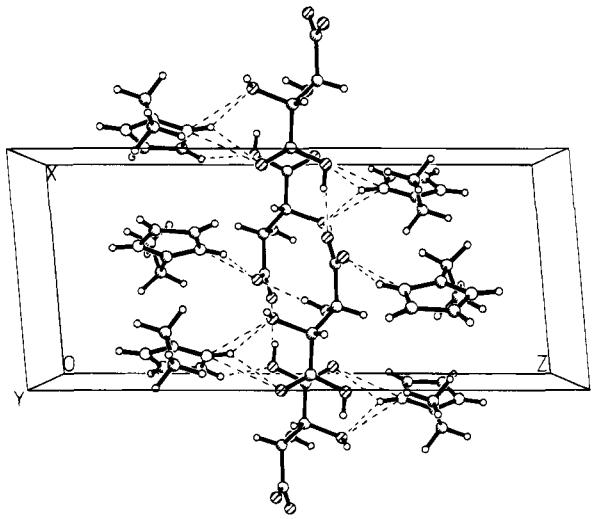

Figure 10. 2-Ethylimidazolium *d*-tartrate, view down *b* axis.

variation in NLO response can be attributed to the choice of cation, to the intermolecular attractions between host and guest, or to the alignment of the guest molecule relative to host lattice. As mentioned earlier, X-ray diffraction analysis of the tartrate salts in this series reveals a significant cross-linked hydrogen bonding network involving tartrate chains interconnected by the imidazolium cations. The hydrogen bonds formed by either host···host or host···guest interactions are listed in Table 2.

Imidazolium *d*-Tartrate (1). From Figure 5, it is observed that the guest molecule is tightly associated with the tartrate lattice near the carboxyl and carboxylate end groups. The host network in this salt is formed by a strong hydrogen bond between the carboxyl and carboxylate end groups, O(1)–H(1B)···O(5) (H···O = 1.868 Å), and the cross-linkage of the hydroxyl groups, O(3)–H(3A)···O(4) (H···O = 2.248 Å). The guest molecule participates in the host network by hydrogen bonding with both protonated nitrogens to carboxylate oxygens, N(1)–H(1A)···O(6) (H···O = 1.854 Å) and

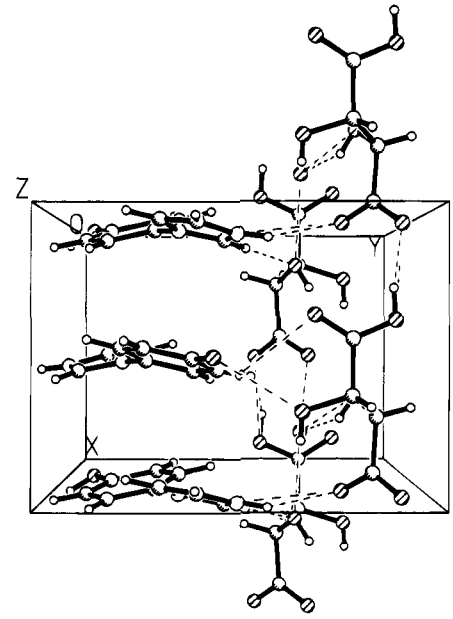

Figure 11. 1-Phenolimidazolium *d*-tartrate, view down *c* axis.

Table 5. Materials Surveyed in This Study

material screened	$I^{2\omega}/I^{2\omega}_{d\text{-tartaric acid}}$
imidazolium *d*-tartrate	2.23
1-vinylimidazolium *d*-tartrate	1.99
1-methylimidazolium *d*-tartrate	1.43
2-methylimidazolium *d*-tartrate	1.37
1-acetophenoneimidazolium *d*-tartrate	1.24
1-phenylimidazolium *d*-tartrate	0.62
2-ethylimidazolium *d*-tartrate	0.44
1-phenolimidazolium *d*-tartrate	0.30
1-benzylimidazolium *d*-tartrate	0.24
2-carboxaldehydeimidazolium *d*-tartrate	0.18
1-benzylimidazole	0.05
imidazole	0
2-methylimidazole	0
2-ethylimidazole	0
α-SiO_2	0.39
d-tartaric acid	1
urea	3
potassium dihydrogen phosphate (KDP)	1

N(3)–H(3B)···O(5) (H···O = 2.238 Å). In addition, the hydrogen on C(4) is weakly interacting with the carboxyl oxygen O(2) and the hydroxyl oxygen O(3) with O···H distances of 2.605 and 2.296 Å, respectively.

1-Vinylimidazolium *d*-Tartrate (2). Figure 6 illustrates the packing network of this salt. The tartrate anions are connected through the carboxyl and carboxylate groups, O(2)–H(2B)···O(5) (H···O = 1.616 Å). However, because this chain runs along a diagonal through the cell, the host chain is defined by the carboxylate to hydroxyl interaction, O(3)–H(3A)···O(6) (H···O = 2.285 Å). The cation participates in four hydrogen bonds with the host lattice. The strongest interaction at 1.826 Å is with the protonated nitrogen group N(3)–H(3B) and the carboxylate oxygen O(6). However, there is an additional interaction with N(3)–H(3B) and O(4) at 2.572 Å. The remaining guest–host interactions are weaker and involve the hydrogen on C(2) with O(2) and O(4) at H···O distances of 2.513 and 2.533 Å, respectively.

2-Methylimidazolium *d*-Tartrate (3). Figure 7 is a view down the *a* axis and clearly illustrates the tartrate chain in the salt. As in the case of **2**, the chain formed by the head to tail arrangement of the carboxyl to carboxylate groups runs along a diagonal through the

cell. Therefore, the host chain is defined by the carboxyl to hydroxyl interaction, O(3)−H(3A)···O(6) (H···O = 2.383 Å). The guest molecule has only two interactions within hydrogen bonding distance. Both nitrogen groups N(1) and N(3) are involved in hydrogen bonding with the carboxyl and carboxylate oxygens, O(6) and O(2), at H···O distances of 2.151 and 1.843 Å, respectively.

1-Methylimidazolium *d*-Tartrate (4). Figure 8 is a view down the *c* axis. In this structure, the carboxyl to carboxylate chain, O(1)−H(1A)···O(6) (H···O = 1.268 Å), runs along the *a* axis and therefore is used to define the host chain. There are cross-linkages of the hydroxyl groups O(3) and O(4) on adjacent tartrate molecules with H···O = 2.109 Å and of the carboxyl group to a hydroxyl group, O(2) to O(4), with a H···O interaction distance of 2.507 Å. The cation participates in hydrogen bonding through four interactions. The strongest hydrogen bond is formed by the N(3)−H(3B)···O(3) interaction with H···O = 2.011 Å. Three weaker interactions are formed between the C(2), C(4), and C(5) carbons and the O(2), O(5), and O(4) oxygens, respectively.

1-Acetophenoneimidazolium *d*-Tartrate (5). Viewed in Figure 9 down the *a* axis, this structure is similar to **1** and **4** in that the chain is defined by a carboxyl-to-carboxylate linkage. The head to tail chain is defined by the O(6)−H(6A)···O(3) bond of 1.787 Å. The relatively large size of the guests molecules prevents any further interactions between the tartrate chains. The cation−anion interactions in this salt are limited to two, the hydrogen bonds between N(3)−H(4B)···O(2) (H···O = 1.665 Å) and C(5)−H(2A)···O(1) (H···O = 2.491 Å). The cation in this salt has an additional donor oxygen group, O(1), which has two weaker interactions with the hydrogens on C(4) and C(5).

2-Ethylimidazolium *d*-Tartrate (6). Figure 10 is a packing view down the *b* axis. The head-to-tail carboxyl-to-carboxylate chains are defined by the O(5A)−H(5AB)···O(2) and O(5)−H(5B)···O(2) bonds with H···O = 1.679 and 1.773 Å, respectively. The tartrate chains are interwoven by four carboxyl- and carboxylate-to-hydroxyl interactions. The cation-to-anion interactions are similar to the other C(2) substituted salts with both nitrogen groups participating in hydrogen bonds with carboxylate and hydroxyl groups.

1-Phenolimidazolium *d*-Tartrate·2H_2O (7). The tartrate chain in this salt (Figure 11) is defined by the carboxyl-to-carboxylate link, O(5)−H(5B)···O(3) (H···O = 1.748 Å), and runs along the *a* axis. There are three hydrogen bonds between guest and host ranging from 1.936 to 2.947 Å. The guest−host lattice in this structure is interrupted by water molecules which are also involved in multiple interactions with the anion.

At this point, we have been unable to identify any obvious correlation in the number or type of hydrogen bonds and the enhancement of SHG efficiency in this series. The influence of hydrogen bonding on the local electronic situation has been found to be significant in other systems and has been proposed to explain the enhanced hyperpolarizability of urea.[35] However, without exact intermolecular distances and more information on the mode of interaction between donor and acceptor in these tartrate salts, it remains unclear what the overall effect of the hydrogen-bond network has on the nonlinear optical properties. Although hydrogen bonding clearly plays a role in the alignment (parallel versus perpendicular) of the imidazolium cations with the tartrate host lattice, we cannot at this point predict the exact cation structural requirements leading to the preferred parallel arrangement. However, it is worth noting that in this extensively hydrogen-bonded system, greater than 70% of the structures adopt the parallel alignment. Despite the uncertainities of the role hydrogen bonding plays in the SHG of these salts, it appears we have successfully engineered high melting points into the salts by exploiting this bonding mode. In particular, salts **1** and **3** have melting points greater than 200 °C.

Comparison to Systematic Observations in Other Chiral Organic Salt Systems. Velsko et al. have performed extensive investigations to identify improved NLO materials based on chiral amino acid and carboxylic acid salts.[12−14] Their work has led to a statistical approach for finding organic salts having certain desirable NLO properties, including SHG efficiencies greater than potassium dihydrogen phosphate (KDP) and noncritical phase matching.[12,14] In the hundreds of chiral salts examined, they have found that only 10% possess powder SHG efficiencies greater than KDP.[14] By comparison, in the imidazolium tartrate salt system discussed here 50% of the salts have SHG efficiencies greater than KDP (see Table 5). This high percentage may be a result of the predominance of the $P2_1$ space group; this space group generally leads to improved SHG efficiencies.[14] In any case, whether the apparent statistically higher SHG efficiencies in the imidazolium salts result from inherent molecular properties of the imidazolium cation or from a preference to crystallize in the $P2_1$ space group, it is clear that this group of chiral organic salts is a fruitful area for new NLO materials.

It is also noteworthy that Velsko et al. could not identify correlations between molecular structure and the NLO properties of their chiral organic salts.[14] However, in many of their salts the counterion to the chiral unit is isotropic, and so no cation−anion directional alignment is possible. This is certainly not the case for the imidazolium tartrate salts where the parallel cation−anion alignment appears to be a prerequisite for optimal SHG efficiency. This correlation between the guest−host molecular structure and the SHG efficiency is an important observation which should be considered when examining the structure of other NLO organic salts, optimizing organic salts for NLO optical applications, and predicting NLO properties with computational methods.

Conclusions

The present crystallographic study of imidazolium tartrate salts has led to the identification of a new series of nonlinear optical materials based on a enantiomeric tartrate host and an imidazolium guest. Of the seven salts presented in this crystallographic investigation, five had improved nonlinear optical properties, i.e., increased SHG efficiencies, over the starting materials. The salient feature of the five improved salts is the nearly parallel alignment of the imidazolium molecular

(35) Chemla, D. S.; Zyss, J. *Nonlinear Optical Properties of Organic Molecules and Crystals;* Academic Press Inc.: New York, 1987; Vol. 1.

plane with the linear tartrate host chain; the other two salts have a nearly perpendicular alignment and exhibit SHG efficiencies attributable to the tartrate alone. To our knowledge this is the first demonstation of this particular type of guest–host optimum alignment. It will be interesting to see if other salt systems containing a linear enantiomeric organic host lattice (e.g., amino acids and other dicarboxylic acids) and an aromatic guest counterion show a similar correlation between SHG efficiency and guest–host alignment.

In addition to the improved SHG properties, these salts possess a number of other favorable characteristics including being colorless, transparent, and readily soluble and having good mechanical properties (e.g., elevated melting points) and high refractive indexes. Furthermore, because the imidazolium guest is easily modified, hydrogen bonding can be used to further tune the physical properties of these NLO materials.

Acknowledgment. Special thanks to N. Heimer for helpful crystallography discussions and to L. Simpson for assistance with the SHG measurements. The Department of Chemistry, United States Air Force Academy is gratefully acknowledged for use of their X-ray diffraction facilities. This work was supported by the Air Force Office of Scientific Research.

Supplementary Material Available: Tables of crystallographic data (22 pages); tables of observed and calculated structure factors (21 pages). Ordering information is given on any current masthead page.

CM940532C